KATHMANDU UNIVERSITY JOURNAL OF SCIENCE, ENGINEERING AND TECHNOLOGY
VOL. 9, No. II, December, 2013, pp 1-14.

MOLECULAR STRUCTURE, MESP, HOMO-LUMO AND VIBRATIONAL ANALYSIS OF β-ASARONE USING DENSITY FUNCTIONAL THEORY

[1]Bhawani Datt Joshi*, [2]Paras Nath Chaudhary

[1]Department of Physics, Siddhanath Sc. Campus, Mahendranager, Tribhuvan University, Nepal
[2]Department of Chemistry, Siddhanath Sc. Campus, Mahendranager, Tribhuvan University, Nepal

*Corresponding author: bdjoshi_007@yahoo.com
Received 09 September, 2013; Revised 29 November, 2013

ABSTRACT
Medicinal plants have always had an important place in the therapeutic armoury of mankind. β-Asarone mainly found in *Acorus calamus L.*, Araceae, is one of the main bioactive constituents of its essential oil. In this communication, we have presented the geometry optimization, molecular electrostatic potential surface, frontier orbital energy gap and vibrational wavenumbers of β-asarone using density functional theory (DFT/B3LYP) method employing 6-311G(d,p) basis set. A complete vibrational assignment has been done on the basis of an isolated molecule. The electronic transition has been calculated in the gas phase as well as in solvent environment (integral-equation formalism polarizable continuum model; IEF-PCM) using TD-DFT/6-31G basis set.

Keywords: β-asarone, vibrational spectroscopy, DFT, MESP, HOMO-LUMO.

INTRODUCTION
Recently, focus on plant research has increased all over the world and a large body of evidence has been collected to show immense potential of medicinal plants used in various traditional systems. Despite the successes that have been achieved over the years with natural products, the interest in them as a platform for drug discovery has waxed and waned in popularity with various pharmaceutical companies as sources of new drug leads.

β-Asarone (*cis*-2,4,5-trimethoxy-1-propenylbenzene) is a major active principle found in *Acorus calamus L.*, of family Araceae, also known as "sweet flag" because of its characteristic sweet odour when fresh. *A. calamus* and the essential oil of its rhizome serve mainly as an insecticide and insect repellent. The rhizomes of *A. calamus* possess insecticidal, larvicidal, antitermite, and larva and insect-repellent properties. In Ayurvedic medicine, the rhizomes are considered to possess antispasmodic, caminative, and anthelmintic properties and are used to cure many disorders, such as epilepsy, and mental diseases [1-9].

In this study, we have used *ab initio* and the density functional theory (DFT) [10] for molecular characterization of the β-asarone, which is gaining more attention in molecular characterization and additional interpretation of the vibrational spectroscopic [11] data to understand the structure-activity relationship. Our past experience shows that the DFT can be used satisfactorily for vibrational analysis of large molecules [12-15]. Hence, the Raman [16] and IR [17] spectra of β-asarone molecule have been analyzed by *ab initio* and DFT. Moreover, we have interpreted the calculated spectra in terms of the potential energy distribution (PED). Information about the geometry and structure of the molecule and its molecular electrostatic potential surfaces (MESP) are useful for understanding the relationship between molecular structure and biological activity.

Further, we have made the calculations for the electronic transition properties of the molecule both in the gas phase as well as in ethanol solvent environment (IEF-PCM model) using TD-DFT/6-31G method [18-20]. The frontier energy orbital gap with the HOMO-LUMO plot has been made to understand the intramolecular charge transition property (ICT) of the molecule.

MATERIALS AND METHODS

Geometry optimization, an important issue in molecular mechanics, was performed as the first task of the computational work for the β-asarone molecule taking the parameters available from Pub Chem Data [21]. It requires in particular the sensitivity of the interaction energy with respect to the change of the molecule's shape which is in general induced by the movement of the nuclei positions. The molecular structure, vibrational frequencies and energies of the optimized geometries of β-asarone were calculated employing the DFT [10] method using Gaussian 09 [22] program package employing 6-311G(d,p) basis set based on Becke's three parameters (local, non-local, Hartree-Fock) hybrid exchange functional with Lee-Yang-Parr correlation functional (B3LYP) [23-25]. The basis set 6-311G(d,p) augmented by 'd' polarization functions on heavy atoms and 'p' polarization functions on hydrogen atoms as well as diffuse functions for both hydrogen and heavy atoms were used [26,27]. The absolute Raman intensities and IR absorption intensities were calculated in the harmonic approximation at the same level of theory as used for the optimized geometries associated with each normal mode, respectively. The normal mode analysis was performed and the PED was calculated along the internal coordinates using localized symmetry. For this purpose, a complete set of 87 internal coordinates were defined using Pulay's recommendations [28,29]. The vibrational assignments of the normal modes were made on the basis of the PED calculated by using the program GAR2PED [30]. Visualization and confirmation of calculated data were done by using the CHEMCRAFT Program [31].

RESULTS AND DISCUSSION

Geometry optimization

Geometry optimization has been taken as the first task taking the parameters (available on Pub Chem Data base). The optimized ground state structure of β-asarone has been given in the Fig. 1. The optimized parameters (parameters for hydrogen atoms are removed) of the ltitle molecule calculated by B3LPY/6-311G(d,p) are listed in the Table 1.

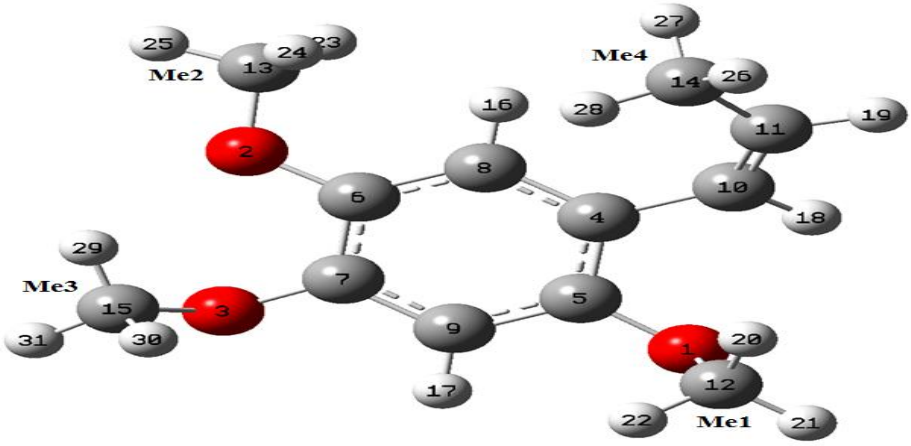

Fig. 1 Optimized structure of β-asarone.

Table 1. Selected optimized paramers of β-asarone by B3LYP/6-311G(d,p) basis set.

Bond lengths (Å)		Bond angles (^{o})		Dihedral angles (^{o})	
R(1,5)	1.38	A(5,1,12)	114.78	D(12,1,5,4)	88.36
R(1,12)	1.43	A(6,2,13)	118.41	D(12,1,5,9)	-93.36
R(2,6)	1.37	A(7,3,15)	116.52	D(5,1,12,20)	-61.29
R(2,13)	1.42	A(5,4,8)	117.60	D(5,1,12,21)	179.52
R(3,7)	1.37	A(5,4,10)	119.48	D(5,1,12,22)	60.62
R(3,15)	1.43	A(8,4,10)	122.79	D(13,2,6,7)	-175.97
R(4,5)	1.40	A(1,5,4)	120.36	D(13,2,6,8)	2.41
R(4,8)	1.41	A(1,5,9)	118.84	D(6,2,13,23)	60.18
R(4,10)	1.47	A(4,5,9)	120.78	D(6,2,13,24)	-62.41
R(5,9)	1.39	A(2,6,7)	116.11	D(6,2,13,25)	178.82
R(6,7)	1.41	A(2,6,8)	124.50	D(15,3,7,6)	-66.26
R(6,8)	1.39	A(7,6,8)	119.37	D(15,3,7,9)	118.00
R(7,9)	1.39	A(3,7,6)	122.25	D(8,4,5,1)	176.36
R(8,16)	1.08	A(3,7,9)	118.56	D(8,4,5,9)	-1.88
R(9,17)	1.08	A(6,7,9)	119.05	D(10,4,5,1)	0.50
R(10,11)	1.34	A(4,8,6)	121.98	D(10,4,5,9)	-177.74
R(10,18)	1.09	A(4,8,16)	118.37	D(5,4,8,6)	1.17
R(11,14)	1.50	A(6,8,16)	119.56	D(5,4,8,16)	-175.46
R(11,19)	1.09	A(5,9,7)	121.19	D(10,4,8,6)	176.88
		A(5,9,17)	119.95	D(10,4,8,16)	0.25
		A(7,9,17)	118.84	D(5,4,10,11)	-146.18
		A(4,10,11)	128.85	D(5,4,10,18)	32.31
		A(4,10,18)	113.84	D(8,4,10,11)	38.19
		A(11,10,18)	117.29	D(8,4,10,18)	-143.32
		A(10,11,14)	128.48	D(1,5,9,7)	-177.12
		A(10,11,19)	116.48	D(1,5,9,17)	1.22
		A(14,11,19)	115.01	D(4,5,9,7)	1.15
				D(4,5,9,17)	179.49
				D(2,6,7,3)	1.67
				D(2,6,7,9)	177.40
				D(8,6,7,3)	-176.80
				D(8,6,7,9)	-1.07
				D(2,6,8,4)	-178.04
				D(2,6,8,16)	-1.45
				D(7,6,8,4)	0.29
				D(7,6,8,16)	176.88
				D(3,7,9,5)	176.25
				D(3,7,9,17)	-2.11
				D(6,7,9,5)	0.36
				D(6,7,9,17)	-178.00

Molecular Electrostatic Potential Surface

In this study, the electrostatic potential (ESP), electron density (ED) and molecular electrostatic potential (MESP) maps have been mapped for β-asarone as shown in Fig. 2. In ESP, the negative potential is localized near the oxygen atoms and reflects by the yellowish blobs, while the positive potential is localized on the rest surface. However, the ED plot of the title molecule shows uniform distribution. The molecular electrostatic potential (MESP), the force acting on a positive test charge located at point through the electrical charge cloud generated through the net charge of molecule (electrons and nuclei), has been a widely used entity in the chemical literature, generally employed as a tool for probing electron rich regions [32-36]. The MESP at a point r in molecular framework with nuclear charges Z_A located at R_A and electron density $\rho(r)$ is given by a relation

$$V(r) = \sum_{A=1}^{N} \frac{Z_A}{|r - R_A|} - \int \frac{\rho(r')}{|r - r'|} d^3r' \quad ,$$

where N is the total number of nuclei in the molecule. The first term on the right hand side of the above equation represent the contribution due to nucleus and second due to electrons, respectively. When the latter contribution overrides the former one, the net MESP attains a negative value, providing information about electron-rich sites.

MESP correlates the total charge distribution with dipole moment, electronegativity, and partial charges and site of chemical reactivity of a molecule. The projections of molecular MESP of β-asarone along the molecular plane and a perpendicular to the plane are given in Fig. 2c. It provides a visual method to understand the relative polarity of a molecule and serves as a useful quantity to explain hydrogen bonding, reactivity and structure-activity relationship of molecules including biomolecules and drugs. It is the potential energy of a proton at a particular location near a molecule. Despite the fact that the molecular charge distribution remains unperturbed through the external test charge (no polarization occurs) the electrostatic potential of a molecule is still a good guide in assessing the molecules reactivity towards positively or negatively charged reactants. Different values of the electrostatic potential at the surface of a molecule appear with the different colours. In general the attractive potential appears in red coloured regions and those of repulsive potential appear in blue. Negative electrostatic potential corresponds to an attraction of the proton by the concentrated electron density in the molecules (from lone pairs, pi-bonds, etc.). Positive electrostatic potential corresponds to repulsion of the proton by the atomic nuclei in regions where low electron density exists and the nuclear charge is incompletely shielded. In the title molecule the negative potentials are located near the oxygen atom of methoxy groups while the positive potentials are located near the hydrogens of the same groups.

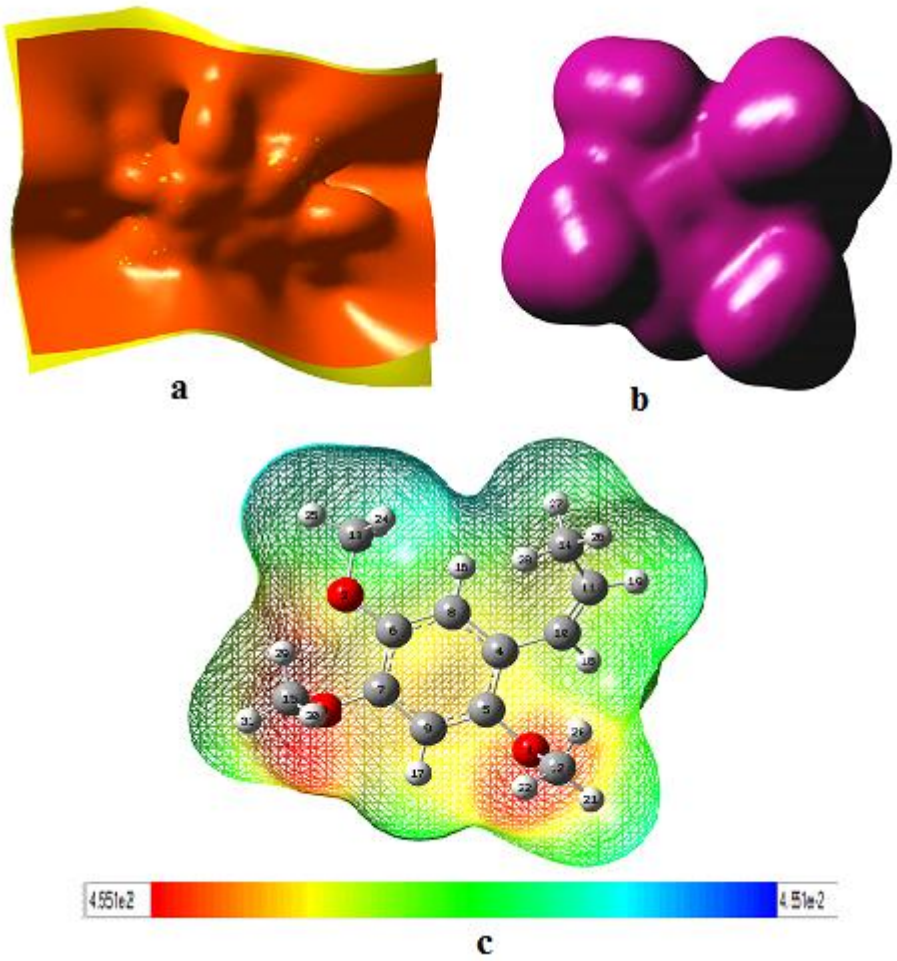

Fig. 2 (a) Electrostatic potential surface (b) electron density and (c) molecular electrostatic potential surface mapped between -4.551e-2 to +4.551e-2.

Electronic Transition and HOMO-LUMO

To understand electronic transitions on terms of energies and oscillator strengths, calculations have been performed in the gas phase as well as in the ethanol solution (IEF-PCM model) using the TD-DFT/6-31G method [18-20]. Both the frontier molecular orbitals, highest occupied molecular orbital (HOMO) and lowest unoccupied molecular orbital (LUMO) are the main orbitals taking part in chemical reaction. The HOMO is the outermost (highest energy) orbital containing electrons that could act as an electron donor. The LUMO is the innermost (lowest energy) orbital that has room to accept electrons and can act as the electron acceptor. According to the frontier molecular orbital theory, the formation of a transition state is due to an interaction between the frontier orbitals (HOMO and LUMO) of reactants [37].

Table 2. Electronic transitions, absorption wavelength λ_{max} (nm), excitation energy (eV), oscillator strengths (f), frontier orbital energies (eV) and dipole moment (Debye) of β-asarone.

Excited State	Calculated								Transition type/ assignments
	Gas Phase				Ethanol				
	λ_{max} (nm)	Transitions	E(ev)	Oscillator strength (f)	λ_{max} (nm)	Transitions	E(ev)	Oscillator strength (f)	
1	273.98	H→L	4.5253	0.1780	275.41	H→L	4.5018	0.2368	$\pi\rightarrow\pi^*$
2	246.04	H+1→L	5.0391	0.1967	246.96	H-1→L	5.0204	0.2351	
3	217.18	H+2→L	5.7089	0.0555	216.27	H-2→L	5.7327	0.0622	
4	205.80	H+3→L	6.0245	0.0312	205.16	H-3→L	6.0434	0.0510	$\pi\rightarrow\pi^*$

E_{HOMO} (eV)	E_{LUMO} (eV)	ΔE (eV)	μ(D)
5.39721713	-0.43219860	4.96501853	3.1778
5.58581931	-0.60020176	4.98561755	4.1239

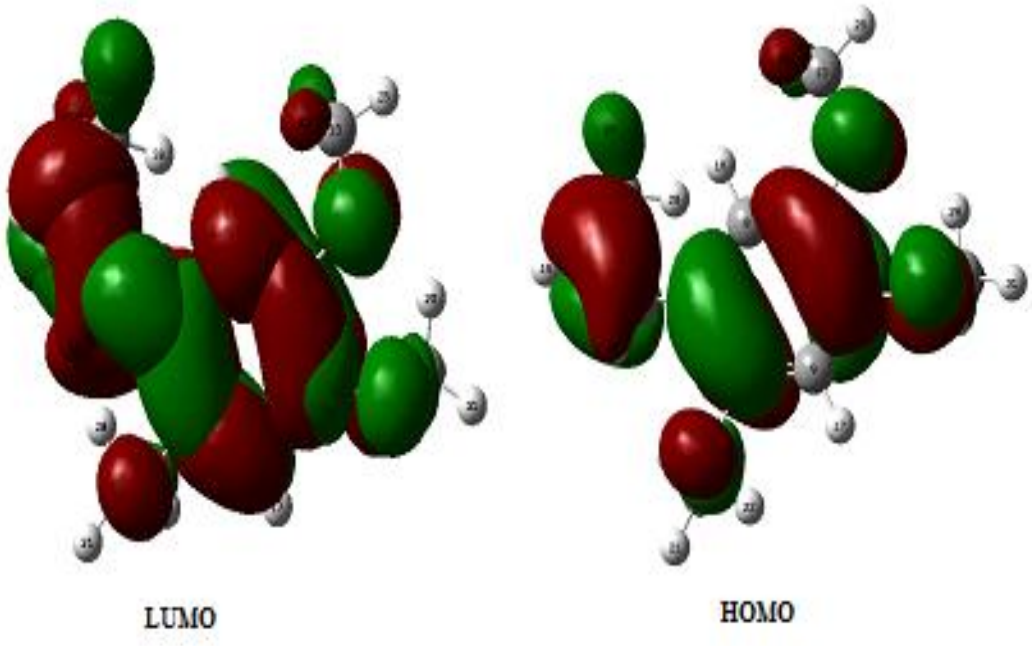

Fig. 3 HOMO and LUMO plot of the β-asarone molecule.

The HOMO-LUMO gap energies along with the energies of different orbits, their wavelengths and oscillator strengths both in the gas phase and the solvent environment are listed in the Table 2. The most important electronic transition in the gas phase was calculated at 273.98 nm with oscillator strength 0.1780. The other transitions were calculated at 246.04 and 217.18 nm with the oscillator strengths 0.1967 and 0.0555, respectively.

The HOMO-LUMO plot has been given in the Fig. 3. The energy of the HOMO is directly related to the ionization potential and the energy of the LUMO is directly related to the electron affinity. High value of HOMO energy is likely to indicate a tendency of the molecule to donate electrons to appropriate acceptor molecule of low empty molecular orbital energy. The lower values of LUMO energy show more probability to accept electrons. From the Fig. 3, it is clearly visible that in the isolated molecule the charge density is shifting from one portion of the

molecule to the other. In case of LUMO the charge is mainly accumulated from the phenyl ring and the *cis* C=C portion. In LUMO the charge is acquired by the same parts significantly.

Vibrational assignments

The title molecule has 31 atoms, hence it gives 87 (= 3N-6) normal modes of vibrations. All the vibrational modes are IR and Raman active. Since the vibrational wavenumbers obtained from the DFT calculations are higher than the experimental wavenumbers, they were scaled down by the wavenumber linear scaling procedure (WLS) [ν_{obs}/ν_{cal} = (1.0087 – 0.0000163 x ν_{cal}) cm^{-1}] of Yoshida *et al.* [38]. All the calculated vibrational wavenumbers reported in this study are the scaled values. The calculated IR and Raman spectra of the β-asarone molecule are given in Figs. 4 and 5, respectively.

The Raman scattering cross sections, $\partial\sigma_j/\partial\Omega$, which are proportional to the Raman intensities, may be calculated from the Raman scattering amplitude and predicted wavenumbers for each normal modes using the relationship [39,40]

$$\frac{\partial\sigma_j}{\partial\Omega} = \left(\frac{2^4\pi^4}{45}\right)\left(\frac{\left(\nu_0-\nu_j\right)^4}{1-\exp\left[\frac{-hc\nu_j}{kT}\right]}\right)\left(\frac{h}{8\pi^2 c\nu_j}\right) S_j$$

where S_j and υ_j are the calculated scattering activities and the predicted wavenumbers, respectively, of the j^{th} normal mode, υ_0 is the Raman excitation wavenumber and *h*, *c* and *k* are the universal constants. The assigned wavenumbers of the vibrational modes calculated at B3LYP level with the basis set 6-311G(d,p) along with their PED are given in Table 3. The assignments of vibrational modes of different functional groups and the phenyl ring have been discussed.

Methyl group vibrations

For a molecule containing a methoxy group, the electronic charge is back donated from the lone pair of electrons on oxygen atom to the σ* orbital of C-H bonds causing weakening of the C-H bonds. This is followed by an increase in C-H bond distance and the decrease in C-H force constant. This can result in enhancement of IR band intensities of the C-H stretching modes [41-43]. The CH_3 group has several modes associated with it, such as; symmetric and asymmetric stretching, bends, rocks, and torsions. Almost the pure asymmetric stretching of Me1, Me2, Me3 and Me4 are calculated in the range 2972-2905 cm^{-1} in the scaled DFT. The symmetric stretching modes for these groups are calculated in the range 2862-2853 cm^{-1}. Both the asymmetric and symmetric deformations of these methyl groups are calculated on the range 1475-1432 cm^{-1}, as listed in the Table 3. The rocking mode of CH_3 group usually appears in the region 1070-1010 cm^{-1} [44]. The rocking modes are calculated below 1192 cm^{-1}.

Table 3 Calculated wavenumbers (cm^{-1}) of β-asarone.

DFT		Intensity		[a]PED (%)
unscaled	scaled	IR	Raman	
3222	3053	3.99	16.31	R[υ(CH)](99)
3198	3031	2.57	47.88	R[υ(CH)](99)
3155	2993	25.53	77.29	υ(CH)(93)
3131	2972	24.80	63.70	Me2[$\upsilon_a(CH_3)$](97)
3129	2970	24.05	66.98	Me3[$\upsilon_a(CH_3)$](98)
3128	2969	20.24	33.79	υ(CH)(81)+Me4[$\upsilon_a(CH_3)$](11)
3119	2961	37.97	77.40	Me1[$\upsilon_a(CH_3)$](100)
3104	2947	6.43	30.85	Me4[$\upsilon_a(CH_3)$](73)+υ(CH)(18)
3091	2935	39.16	36.15	Me3[$\upsilon_a(CH_3)$](99)
3059	2906	40.81	27.24	Me2[$\upsilon_a(CH_3)$](99)
3058	2905	35.96	17.68	Me1[$\upsilon_a(CH_3)$](99)
3054	2902	25.35	76.00	Me4[$\upsilon_a(CH_3)$](99)
3010	2862	74.08	81.57	Me3[$\upsilon_s(CH_3)$](98)
3006	2859	37.31	136.17	Me4[$\upsilon_s(CH_3)$](98)
3001	2854	37.13	64.87	Me2[$\upsilon_s(CH_3)$](89)+Me1[$\upsilon_s(CH_3)$](30)
2999	2853	63.84	35.56	Me1[$\upsilon_s(CH_3)$](88)+Me2[$\upsilon_s(CH_3)$](30)
1700	1653	0.92	606.30	υ(C=C)(48)+[ρ(15)+δ(11)][HC=CH)](11)+δ(C4C10C11)(17)+ρ(C4C10C11)(15) +υ(C11C14)(5)+R[υ(C4C10)](5)
1641	1597	19.27	545.78	R[υ(CC)(61)+δ_a(19)+δ_{in}(CH)(13)]
1596	1554	17.01	76.72	R[υ(CC)(76)+δ'_a(9)]
1534	1496	214.99	12.18	R[υ(CC)(35)+δ_{in}(CH)(26)+υ(CO)(23)]
1512	1475	9.73	37.88	[δ_a(80)+δ'_a(9)+ρ'(8)][Me3(CH_3)]
1507	1470	53.76	17.12	[δ_a(76)+ρ'(7)][Me2(CH_3)]
1504	1467	12.96	32.36	[δ'_a(46)+δ_a(35)+ρ'(7)][Me1(CH_3)] +δ_a[Me2(CH_3)](7)
1494	1458	15.56	52.03	[δ'_a(41)+δ_a(9)][Me4(CH_3)]+δ'_a[Me2(CH_3)](39)
1492	1456	8.31	139.50	δ_a[Me4(CH_3)](25)+δ_s[Me2(CH_3)](20)+[δ_s(16)][Me3(CH_3)]+δ_s[Me1(CH_3)](11)
1492	1455	3.45	31.03	δ'_a[Me2(CH_3)](49)+[δ'_a(17)+δ_a(14)][Me4(CH_3)]
1489	1453	2.21	26.08	[δ_a(35)+δ'_a(29)[Me1(CH_3)]+[δ_a(11)+δ'_a(8)][Me4(CH_3)]
1487	1451	9.25	39.55	[δ_a(25)+δ'_a(22)[Me4(CH_3)]+[δ_a[(22)+δ'_a(8)][Me1(CH_3)]
1485	1449	12.28	34.94	[δ'_a(71)+δ_a(10)+ρ(5)][Me3(CH_3)]+δ_s[Me1(CH_3)](7)
1479	1443	0.09	12.21	δ_s[Me2(CH_3)](50)+δ_s[Me1(CH_3)](32)+δ'_a[Me3(CH_3)](5)
1467	1432	34.26	19.67	δ_s[Me3(CH_3)](55)+δ_s[Me1(CH_3)](23)+δ_s[Me2(CH_3)](5)
1439	1405	33.77	74.11	[ρ(26)+δ(18)][HC=CH]+R[υ(C11C14)(11)+υ(C4C10)(8)+υ(CC)(5)]+δ_s[Me4(CH_3)](14)+δ(C4C10C11)(6)
1419	1386	54.96	26.10	R[υ(CC)](32)+ρ[HC=CH)](11)+δ_s[Me4(CH_3)](9)+δ_s[Me3(CH_3)](7)
1404	1371	7.07	44.01	δ_s[Me4(CH_3)](73)+ρ[HC=CH)(14)]
1337	1308	48.54	376.23	R[υ(CC)(35)+υ(CO)(34)]+ρ[HC=CH)](7)
1321	1292	49.97	146.33	[δ(27)+ρ(21)][HC=CH]+R[υ(CC)](39)
1274	1248	88.99	27.64	[δ(37)+ρ(35)][HC=CH)]+R[δ_{in}(CH)](8)
1263	1237	4.21	21.00	[δ(37)+ρ(34)][HC=CH)]+R[δ_{in}(CH)](12)
1234	1209	197.67	23.32	R[υ(CO)(28)+δ_{trig}(14)]+[ρ(9)+δ(5)](HC=CH)+υ(C13O)(6)+ρ'[Me3(CH_3)](

				6)
1216	1192	43.38	28.80	[ρ'(33)+ρ(10)][Me1(CH_3)]+ρ'[Me3(CH_3)](12)+R[υ(CO)(15)+δ_{in}(CH)(9)]
1212	1188	4.62	12.45	[ρ'(48)+ρ(16)+δ_a(5)] [Me2(CH_3)]+ρ'[Me3(CH_3)](10)
1197	1174	65.66	13.75	(ρ'+ρ)[Me3(CH_3)](29)+(ρ'+ρ)[Me1(CH_3)](22)+R[δ_{trig}](9)+ρ'[Me2(CH_3)](5)
1176	1153	105.13	11.90	R[δ_{in}(CH)(29)+υ(CO)(20)]+ρ'[Me3(CH_3)](8)+υ(C15O)(8)+υ(C12O)(5)
1172	1149	1.33	11.07	[ρ(65)+ρ'(25)][Me2(CH_3)]
1169	1147	16.82	11.22	[ρ(70)+ρ'(24)][Me1(CH_3)]
1169	1146	0.28	17.37	[ρ(67)+ρ'(21)][Me3(CH_3)]+ρ[Me2(CH_3)](5)
1139	1118	50.07	58.43	R[υ(C4C10)(15)+υ(CO)(14)+δ_{trig}(8)]+υ(C13O)(10)+υ(C12O)(8)
1097	1078	14.56	4.20	[δ(33)+ρ(18)(HC=CH)+δ(C4C10C11)(12)+[ρ(11)+ρ'(9)][Me4(CH_3)]+R[υ(C11C14)](6)
1061	1042	80.81	4.96	υ(C13O)(54)+υ(C12O)(11)+R[υ(CC)(8)+δ_{in}(CH)(7)+δ_{trig}(5)]+υ(C15O)(5)
1060	1041	16.81	19.86	[ρ(36)+ρ'(34)+δ'_a(5)][Me4(CH_3)]+δ[oop(HC=CH)](10)+τ(C10C11)(7)+δ[oop(C4C10C11C14)](7)
1037	1019	85.69	47.18	υ(C15O)(42)+υ(C12O)(40)+R[δ_{trig}](5)
1010	994	2.15	150.81	δ[oop(HC=CH)](79)+τ(C10C11)(10)
996	979	14.58	39.90	υ(C15O3)(21)+υ(C12O)(19)+υ(C13O)(9)+R[υ(C4C10)(6)+υ(CO)(6)+δ_a(5)]
933	918	10.27	19.57	R[υ(C11C14)](56)+δ(C4C10C11)(10)+ρ'[Me4(CH_3)](8)+υ(C=C)(6)+ρ[Me4(CH_3)](5)
906	892	26.74	11.69	R[oop(CH)(77)+τ'_a(6)]
875	862	14.28	7.68	R[oop(CH)(54)+puck(19)+oop(CH)(11)]
855	843	22.20	23.11	[ρ(22)+δ(11)](HC=CH)+R[υ(CO)(12)+υ(C4C10)(6)]
797	786	19.09	59.86	τ(C10C11)(30)+R[oop(C4C10)(15)+oop(C5O)(13)+puck(8)+τ_a(7)]
751	742	9.27	132.15	R[υ(CC)(27)+δ'_a(20)+ δa(6)+υ(CO)(5)]+τ(C10C11)(7)
741	732	0.08	34.71	R[puck(40)+oop(CO)(37)]
717	708	13.03	86.91	R[oop(CO)(32)+τ_a(17)]+τ(C10C11)(21)
681	673	9.06	10.46	R[puck(26)+oop(CO)(18)+δ_{trig}(8)+ρ(C4C10C11)(7)+δ(C4C10C11)(5)
644	637	12.20	13.23	R[δ_{trig}](16)+δ_{in}(CO)(14)+υ(C4C10)(10)+δ_a(7)+δ_{in}(C4C10)(5)]+ρ(C4C10C11)(8)
613	607	5.94	72.96	R[δ_{in}(CO)(38)+δ(C6C13O)](8)+ρ(C4C10C11)(9)+ δ(C4C10C11)(8)
531	527	9.28	181.89	δ[oop(C4C10C11C14)](28)+R[oop(C4C10)(21)+τ_a(9)+δ(C5C12O)(8)]+τ(C4C10)(6)
509	505	2.46	17.05	R[oop(CO)(41)+τ'_a(27)+δ(C7C15O)(10)]
495	491	3.43	88.39	R[δ'_a](19)+δ(C6C13O)(16)+puck(5)]+δ[oop(C4C10C11C14)](9)
434	431	3.98	36.90	R[δ_a](16)+δ(C6C13O)(15)+τ'_a(12)+τ_a(7)+oop(CO)(5)]
405	402	1.55	66.16	δ[oop(C4C10C11C14)](35)+R[puck(13)+oop(CO)(6)+τ_a(6)+oop(C4C10)(5)]+τ(C10C11)(11)
377	374	2.32	17.94	R[δ_a](19)+δ_{in}(CO)](13)+δ(C6C13O)(5)]+δ(C4C10C11)(15)+[δ(13)+ρ(8)](HC=CH)
346	344	6.49	128.97	R[δ(C7C15O)(16)+puck(14)+τ'_a(13)+τ_a(13)+oop(CH)(8)+δ_{in}(CO)(6)+δ(C5C12O)(5)]
308	307	4.30	57.75	R[δ_{in}(CO)(38)+δ'_a(8)+(C6C13O)(8)]+τ(CO)(8)
287	286	1.27	21.63	τ(C13O)(32)+R[δ(C5C12O)(8)+oop(CH)(6)+τ'a(7)]+[δ(7)+ρ(7)](HC=CH)
273	272	2.77	95.96	R[δ_{in}(CO)(17)+δ_{in}(C4C10)(12)+δ(C7C15O)(7)]+δ(C4C10C11)(8)+[δ(8)+ρ

				(7)](HC=CH)
240	239	0.44	22.69	τ(C13O)(45)+[ρ(7)+δ(7)](HC=CH)+τ(C11C14)(6)+ρ(C4C10C11)(5)+ R[oop(C6O)](5)
210	209	1.49	45.17	R[oop(CO)(26)+τ'_a(11)+δ(C7C15O)(7)+δ(C5C12O)(6)+δ_{in}(C4C10)(5)]+τ(C11C14)(12)+δ[oop(C4C10C11C14)](6)
191	191	1.17	221.18	τ(C11C14)(27)+τ(C12O)(14)+R[puck(8)+δ(CO)(5)]+τ(C15O)(5)
178	177	2.15	58.65	τ(C12O)(61)+τ(C11C14)(12)+R[δ_{in}(C5O)](8)
170	169	0.33	14.74	τ(C15O)(32)+τ(C7O)(8)+R[oop(C4C10)(7)+oop(CO)(5)]+δ[oop(C4C10C 11C14)](6)+τ(C10C11)(5)
165	165	1.59	67.71	τ(C15O)(20)+τ(C6O)(15)+R[oop(CO)](16)+τ'_a(7)+δ(C5C12O)(5)]
133	133	0.88	158.45	ρ(C4C10C11)(16)+[ρ(11)+δ(10)[HC=CH]+R[δ_{in}(C4C10)(11)+τ_a](11)+τ(C 6O)(10) +(C11C14)(7)
119	118	1.03	321.78	τ(C11C14)(17)+δ[oop(C4C10C11C14)](9)+δ(C4C10C11)(9)+R[δ(C6O)(8)+δ_{in}(C4C10)(8)+oop(C4C10)(5)]+[δ(6)+ρ(5)][HC=CH]
88	88	2.69	261.49	τ(C6O)(15)+R[τ_a(12)+δ_{in}(C4C10)(6)]+τ(C11C14)(12)+τ(C5O)(10)+τ(C4C 10)(8) +ρ(C4C10C11)(5)+τ(C13O)(5)
77	77	2.52	343.75	τ(C7O)(34)+τ(C6O)(21)+R[δ_{in}(C7O)(5)+δ(C7C15O)(5)]+τ(C13O)(8)+τ(C 15O)(5) +τ(C5O)(5)
69	69	2.86	956.16	τ(C7O)(43)+R[δ(C7C15O)(7)+τ'_a(6)+δ_{in}(C7O)(5)]+τ(C6O)(8)+τ(C4C10)(5)
51	51	2.36	610.95	τ(C5O)(53)+R[τ_a](19)+τ(C6O)(5)
42	42	0.60	4193.1	τ(C4C10)(50)+τ(C11C14)(8)+ρ(C4C10C11)(7)+[δ(6)+ρ(5)][HC=CH)]+τ(C5O)(5)

Proposed assignments and potential energy distribution (PED) for vibrational normal modes.
Types of vibration: ν, stretching; δ, deformation (bending), scissoring; oop, out-of-plane bending; ρ, rocking; τ, torsion.
[a]Potential energy distribution (contribution ≥ 5).

HC=CH vibration

The C-H stretching vibration of this HC=CH group is calculated at 2993/2969 cm-1 with low contribution and intensity 20.24/33.79 and 25.53/77.29 units in the IR/Raman spectra, respectively. The C=C stretching is calculated at 1653 cm^{-1} with low intensity of 0.92 units in the IR spectrum and very high intensity of 606.30 units in the Raman spectrum, respectively. The highly mixed HC=CH rocking mode is calculated at 1405 cm^{-1} with IR intensity of 33.77 units and Raman intensity of 74.11 units, respectively.

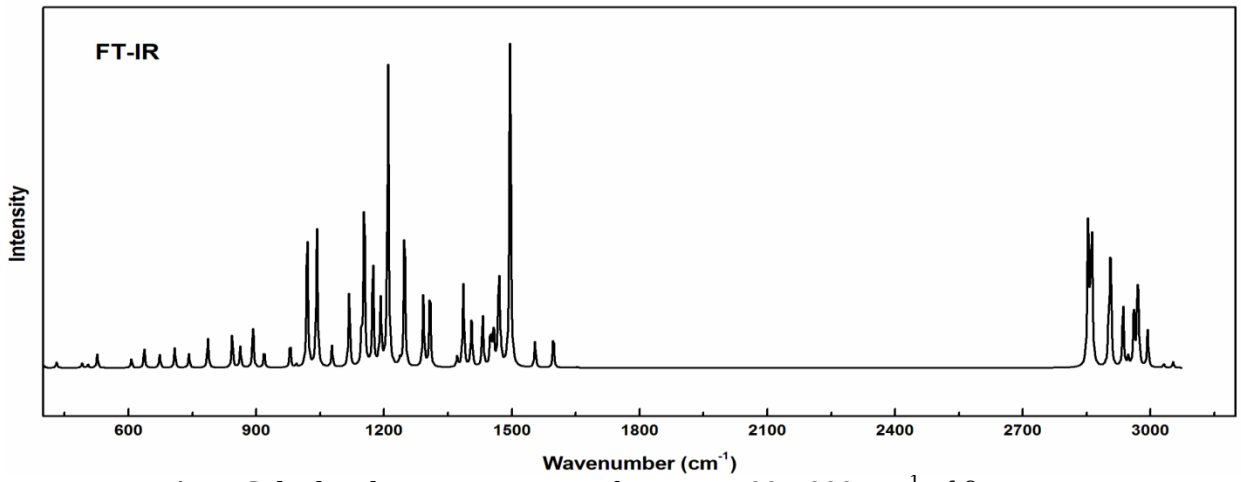

Fig. 4 Calculated FT-IR spectra in the range 400-4000 cm^{-1} of β-asarone.

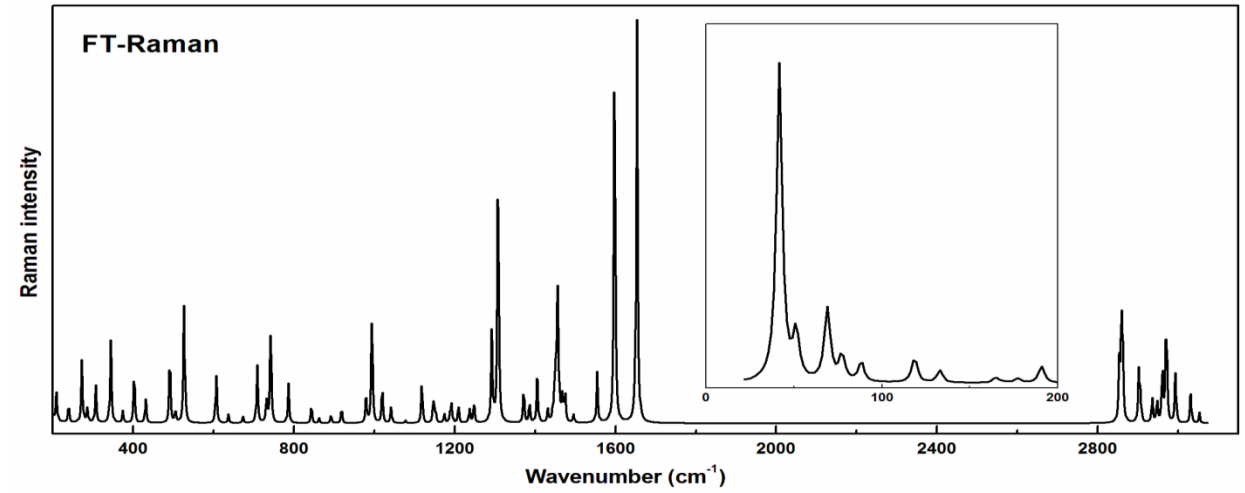

Fig. 5 Calculated FT-Raman spectra in the range200-3200 cm^{-1} of β-asarone.

Phenyl ring vibration

The carbon hydrogen stretching vibrations give rise to bands in the region 3100-3000 cm^{-1} in all the aromatic compounds [45]. The ring C-H stretching vibrations appear to be very weak. This is due to steric interaction that induces effective conjugation and charge carrier localization resulting in twisted phenyl ring [46]. In this region, the bands are not affected appreciably by the nature of the substituent. There are two C-H moieties with the phenyl ring. The pure C-H stretching vibrations are calculated at 3053 and 3031 cm^{-1} with very weak intensity in the IR and medium intensity in the Raman spectra, respectively. These are localized modes and have almost 100% contribution in the potential energy distribution. The C-H in-plane deformation is calculated at 1153 cm^{-1} with very high intensity of 105.13 units in the IR and weak intensity of 11.90 units in the Raman spectrum, respectively. The C-H out-of-plane deformation is calculated at 892 and 862 cm^{-1}. The phenyl ring asymmetric, symmetric deformations and puckering modes are calculated in the coupled vibrations below a range of 650 cm^{-1}. The phenyl ring torsional modes are observed as strongly coupled vibrations in lower wavenumber range (below 500 cm^{-1}).

There three methoxyl groups connected with the phenyl group, the C-O stretching vibrations associated with the ring are calculated at 1209 cm^{-1} and below this value in the mixed modes. The C-O in-plane bending is calculated at 607, 286 and 272 cm^{-1} in the highly mixed modes. The C-O out-of-plane bending vibrations are calculated at 708, 505 and 209 cm^{-1}, respectively. The C4-C10 stretching vibration is calculated at 1118 cm^{-1} with medium intensity bands in the R and Raman spectra.

CONCLUSION

The equilibrium geometries and harmonic vibrational wavenumbers of all the 87 normal modes of the Asarone molecule were determined and analyzed at DFT (B3LYP) level of theory employing the 6-311G(d,p) basis set. These calculated vibrational assignments along with the electronic transitions are important to understand the molecular structure and biological activity of the title molecule. Information about the size, shape, charge density distribution and structure-activity relationship of the title molecule has been obtained by mapping electron density isosurface with ESP and MESP. The electronic transition have been calculated in the gas phase as well as in ethanol environment (IEF-PCM model) using TD-DFT//B3LYP/6-31G basis set shows the charge transfer within the molecule. HOMO-LUMO made very clearly the involvement of charge transfer between the donor and acceptor groups.

REFERENCES

[1] Zou X, Liu S L, Zhou J Y, Wu J, Ling B F, Wang R P, Beta-asarone Induces LoVo Colon Cancer Cell Apoptosis by Up-regulation of Caspases through a Mitochondrial Pathway in vitro and in vivo, *Asian Pacific J. Cancer Prev*, 13 (10) 5291.

[2] Shenvi S, Vinod, Hegde R, Kush A & Chandrasekara Reddy G, A unique water soluble formulation of β-asarone from sweet flag (*Acorus calamus* L.) and its in vitro activity against some fungal plant pathogens, *J. Med. Plants Res.*, 5 (20) (2011) 5132.

[3] Asha D S & Ganjewala D, Antimicrobial activity of *Acorus calamus* (L.) rhizome and leaf extract, *Act. Biol. Szeg.*, 53 (1) (2009) 45.

[4] Björnstad K, Helander A, Hultén P, & Beck O, Bioanalytical Investigation of Asarone in Connection with *Acorus calamus* Oil Intoxications, *J. Anal. Toxicol.*, 33 (2009) 604.

[5] Singh C, Jaiswal U & P. Singh P, *Acorus calamus* "sweet flag": an overview of oil composition, biological activity and usage, *J. Med. Aromat. Plant Sc.*, 23 (2001) 687.

[6] Deng C, Lin S, Huang T, Duan G, & Zhang X, Development of gas chromatography/mass spectrometry following headspace solid-phase micro extraction for fast determination of asarones in plasma *Rapid Commun. Mass Spectrom.*, 20 (2006) 2120.

[7] Hasheminejad G & Caldwell J, Genotoxicity of the alkenylbenzenes alpha- and beta-asarone, myristicin and elimicin as determined by the UDS assay in cultured rat hepatocytes, *Food Chem. Toxicol.*, 32 (1994) 223.

[8] Lee Y S, Kim J, Lee S G, Sang-Chul Shin S C & Parket I K, Fumigant antifungal activity of essential oil components from Acorus gramineus against three phytopathogenic fungi, *Antifun. Act. Essent. Oil Comp.*, 63(2008) 503.

[9] Raina R V, Srivastava S K & Syamasunder K V, Essential oil composition of *Acorus calamus* L. from the lower region of the Himalayas, *Flavour Fragrance J.*, 18 (2003) 18.

[10] Hohenberg P & Kohn W, Inhomogeneous Electron Gas, *Phys. Rev. B*, 136B (1964) 864.

[11] Chamers J M & Griffiths P R, *Handbook of Vibrational Spectroscopy*, John Wiley and Sons, New York, 2002.
[12] Joshi B D, Srivastava A, Tandon P & Jain S, Molecular structure, vibrational spectra and HOMO, LUMO analysis of yohimbine hydrochloride by density functional theory and *ab inito* Hartree-Fuck calculations, *Spectrochim. Acta .A*, 82 (2011) 270.
[13] Joshi B D, Srivastava A, Tandon P & Jain S, Molecular characterization of yohimbine hydrochloride using vibrational spectroscopy and quantum chemical calculations, *BIBECHANA*, 8 (2012)73.
[14] Joshi B D, Srivastava A,Honorato S B, Tandon P, Pessoa O D L, Fechine P B A & Ayala A P, Study of molecular structure, vibrational, electronic and NMR spectra of oncocalyxone A using DFT and quantum chemical calculations, *Spectrochim. Acta A*, 113 (2013) 367.
[15] Srivastava A, Joshi B D, Tandon P, Ayala A P, Bansal A K &, Grillo D, Study of polymorphism in anti cancerous imatinib mesylate: A quantum chemical approach using electronic and vibrational spectra, *Spectrochim. Acta A*, 103 (2013) 325.
[16] Crupi V, Majolino D, Mondello R, Migliardo P & Venuti V, FTIR spectroscopy: a powerful tool in pharmacology, *J. Pharm. Biomed. Anal.*, 29 (2002) 1149.
[17] Fini G, Applications of Raman spectroscopy to pharmacy, *J. Raman Spectrosc*., 35 (2004) 335.
[18] Miertus S & Tomasi J, Approximate evaluations of the electrostatic free energy and internal energy changes in solution processes, *Chem. Phys*., 65 (1982) 239.
[19] Casida M E, Casida K C & Salahub D R, Excited-state potential energy curves from time-dependent density-functional theory: A cross section of formaldehyde's $^1A_1$ manifold, *Int. J. Quan. Chem.*, 70 (1998) 933.
[20] Stratmann R E, Scuseria G E & Frisch M J, An efficient implementation of time-dependent density-functional theory for the calculation of excitation energies of large molecules, *J. Chem. Phys*., 109 (1998) 8218.
[21] PubChem Structure Search, *pubchem.ncbi.nlm.nih.gov*, NCBI (online).
[22] Frisch M J, Trucks G W, Schlegel H B, Scuseria G E, Cheeseman J R, *et al*., *Gaussian 09, Revision*, Gaussian, Inc., Wallingford CT, 2009.
[23] Lee C T, Yang W & Parr R G, Development of the Colle-Salvetti correlation-energy formula into a functional of the electron density, *Phys. Rev*., 37B (1988) 785.
[24] Parr R G & Yang W, Density Functional Theory of Atoms and Molecules, Oxford University Press, New York, 1989.
[25] Becke A D, Density-functional thermochemistry. III. The role of exact exchange, *Chem. Phys*., 98 (1993) 5648.
[26] Petersson G A, Al-Laham M A, A complete basis set model chemistry II. Open-shell systems and the total energies of the first-row atoms, *J. Chem. Phys*., 94 (1991) 6081.
[27] Petersson G A, Bennett A, Tensfeldt T G, Allaham M A, Shirley W A & Mantzaris J, A complete basis set model chemistry I. The total energies of closed-shell atoms and hydrides of the first-row elements, *J. Chem. Phys.*, 89 (1988) 2193.
[28] Pulay P, Fogarasi G, Pang F & Boggs J E, Systematic ab initio gradient calculation of molecular geometries, force constants, and dipole moment derivatives, *J. Am. Chem. Soc.*, 101 (1979) 2550.

[29] Fogarasi G, Zhou X, Taylor P W & Pulay P, The calculation of ab initio molecular geometries: efficient optimization by natural internal coordinates and empirical correction by offset forces, *J. Am. Chem. Soc.*, 114 (1992) 8191.
[30] Martin J M L & Alsenoy C V, Gar2ped, University of Antwerp, 1995.
[31] Zhurko G A & Zhurko D A, <http://www.chemcraftprog.com> Chemcraft, 2005.
[32] Politzer P & Truhlar D G, *Chemical Applications of Atomic and Molecular Electrostatic Potentials*, Plenum, New York, 1981.
[33] Pingale S S, Molecular Electrostatic Potentials Concepts and Applications, *Phys. Chem. Chem. Phys.*, 13 (2011) 15158.
[34] Politzer P, Grice M E, Murray J S & Seminario J M, Anomalous Stabilizing and Destabilizing Effects in Some Cyclic p-Electron Systems, *Can. J. Chem*., 71 (1993) 1123.
[35] Suresh C H, Alexander P, Vijayalakshmi K P, Sajith P K & Gadre S R, Use of molecular electrostatic potential for quantitative assessment of inductive effect, *Phys. Chem. Chem. Phys.*, 10 (43) (2008) 6492.
[36] Balnarayan P & Gadre S R, Topography of molecular scalar filds. I. Algorithm and Poincare-Hopf relation, *J. Chem. Phys.*, 119 (2003) 5037.
[37] Issa R M, Awad M K & Atlam F M, Quantum chemical studies on the inhibition of corrosion of copper surface by substituted uracils, *Appl. Surf. Sci*., 255 (2008) 2433.
[38] Yoshida H, Takeda K, Okamura J, Ehara A & Matsurra H, A new approach to vibrational analysis of large molecules by density functional theory; wavenumber linear scaling method, *J. Phys. Chem*., 106 (2002) 3580.
[39] Guirgis G A, Klaboe P, Shen S, Powell D L, Gruodis A, Aleksa V, Nielsen C J, Tao J, Zheng C & Durig J R, Spectra and structure of silicon-containing compounds. XXXVI-Raman and infrared spectra, conformational stability, *ab initio* calculations and vibrational assignment of ethyldibromosilane, *J. Raman. Spectrosc*., 34 (2003) 322.
[40] Polavarapu P L, *Ab initio* vibrational Raman and Raman optical activity spectra, *J. Phys. Chem*., 94 (1990) 8106.
[41] Rumi M & Zerbi G, Conformational dependence of vibrational and molecular nonlinear optical properties in substituted benzenes: the role of π-electron conjugation and back-donation, *J. Mol. Struct*., 509 (1999) 11.
[42] Anderson G M, Kollman P A, Domelsmith L N & Houk K N, Methoxy group nonplanarity in o-dimethoxybenzenes. Simple predictive models for conformations and rotational barriers in alkoxyaromatics, *J. Am. Chem. Soc*., 101 (1979) 2344.
[43] Tommasini M, Castiglioni C, Del Zoppo M & Zerbi G, Relationship between infrared and Raman intensities in molecules with polarized *π* electrons, *J. Mol. Struct*., 480 (1999) 179.
[44] Silverstein R M & Webster F X, *Spectroscopic Identification of Organic Com-pounds*, sixth ed., John Wiley & Sons Inc., New York, 2003.
[45] Smith B, *Infrared Spectral Interpretation. A Systematic Approach*, CRC Press, Washington, DC, 1999.
[46] James C, Pettit G R, Nielsen O F, Jayakumar V S & Hubert Joe I, Vibrational spectra and *ab initio* molecular orbital calculations of the novel anti-cancer drug combretastatin A-4 prodrug *Spectrochim. Acta A*, 70 (2008) 1208.